# Preasymptotic Nature of Hadron Scattering vs Small-$x$ HERA Data

P. M. Nadolsky, S. M. Troshin, N. E. Tyurin
Institute for High Energy Physics
Protvino, Moscow Region, 142284 Russia

**Abstract**

We emphasize that recently observed regularities in hadron interactions and deep-inelastic scattering are of preasymptotic nature and it is impossible to make conclusions on the true asymptotic behavior of observables without unitarization procedure. Unitarization is important and changes scattering picture drastically.

The existence of the regular calculational method for hard processes inspires one to promptly apply the parton model also to calculation of cross sections for soft processes. The problems of this extension are notorious. They are related both to the increase of the effective coupling constant and the phenomenon of the spontaneous breaking of chiral symmetry. The chiral symmetry breaking results, in particular, in generation of large quark masses and in appearance of quark condensates. Nevertheless, the leading logarithm approximation in the framework of perturbative QCD was used to derive several results for soft processes, in particular, the value of hard Pomeron intercept $1 + \Delta \simeq 1.5$ [1]. This value seems to find confirmation in the deep–inelastic scattering data at small $x$, obtained recently at HERA [2].

Having in mind the new data from HERA and much discussion around hard Pomeron [2], in this note we would like to emphasize that the scattering of hadrons at energies lower than $\sqrt{s} \sim 0.5$ TeV is of preasymptotic nature. Thus, at this range of energies we have not any restrictions on the possible behavior of cross–sections, following from asymptotic theorems.

In general, only an approach, explicitly taking into account the unitarity, allows one to accurately distinguish between the asymptotic and preasymptotic regimes of scattering. In Refs. [3, 4] we have used the notions of

effective chiral quark models for the description of elastic scattering at small and large angles. This description is based on the results of the effective Lagrangian approach and accounts various aspects of hadron dynamics. For example, massive quarks appear as quasiparticles, i.e. as current quarks surrounded by the clouds of quark–antiquark pairs of different flavors. Besides mass, quark acquires non-trivial internal structure and finite size. Quark radii are determined by the radii of the clouds. Strong interaction radius of the massive quark $Q$ is determined by its Compton wavelength:

$$r_Q = \xi/m_Q, \tag{1}$$

where the constant $\xi$ is universal for different flavors. The quark formfactor $F_Q(q)$ is taken in the dipole form, viz

$$F_Q(q) \simeq (1 + \xi^2\vec{q}^2/m_Q^2)^{-2}, \tag{2}$$

and the corresponding quark matter distribution $d_Q(b)$ is of the form [4]

$$d_Q(b) \propto \exp(-m_Q b/\xi). \tag{3}$$

Quantum numbers of the constituent quarks are the same as the quantum numbers of current quarks due to conservation of the corresponding currents in QCD (we do not concern here the axial-vector currents related to spin degrees of freedom).

A common feature of chiral models [5] is the representation of a baryon as an inner core, carrying the baryonic charge, and an outer condensate, surrounding this core [6]. Following these observations, it is natural to represent a hadron as consisting of the inner region, where constituent quarks are located, and the outer region, filled with the quark condensate [4]. This picture implies that the first stage of the hadron collision is determined by the overlap and interaction of peripheral condensates. In the overlapping region the condensates interact and, as a result, virtual massive quarks appear. In other words, nonlinear field couplings transform kinetic energy of condensates into the internal energy of dressed quarks (see the arguments for this mechanism in [7] and references therein for the earlier works). Of course, the number of such quarks fluctuates. The average number of quarks is proportional to the convolution of the condensate distributions $D_c^H$ of colliding hadrons:

$$\tilde{N}(s,b) \simeq \mathcal{N}(s) \cdot D_c^A \otimes D_c^B, \tag{4}$$

where the function $\mathcal{N}(s)$ is determined by thermodynamics of the kinetic energy transformation. To estimate $\mathcal{N}(s)$ one may assume that it has maximal possible energy dependence,

$$\mathcal{N}(s) \simeq \kappa \frac{(1 - \langle x_Q \rangle)\sqrt{s}}{m_Q}, \tag{5}$$

where $\langle x_Q \rangle$ is the average fraction of the energy carried by constituent quarks, $m_Q$ is the mass of the constituent quark.

In the model the constituent quarks, located in the central part of the hadron, are supposed to scatter in a quasi-independent way both by the produced virtual massive quarks and by other constituent quarks. The scattering amplitude of the constituent quark, smeared over its longitudinal momentum, may be then represented in the form

$$\langle f_Q(s,b) \rangle = [\tilde{N}(s,b) + N - 1] \langle V_Q(b) \rangle, \tag{6}$$

where $N = N_1 + N_2$ is the total number of constituent quarks in colliding hadrons, and $\langle V_Q(b) \rangle$ is the averaged amplitude of single quark-quark scattering.

In this approach the elastic scattering amplitude is constructed as a solution of the equation [8]

$$F = U + iUDF, \tag{7}$$

which is presented here in the operator form. This equation allows one to satisfy unitarity, provided the inequality

$$\text{Im } U(s,b) \geq 0 \tag{8}$$

is fulfilled. The function $U(s,b)$ (generalized reaction matrix) [8] — the basic dynamical quantity of this approach — is chosen as a product of the averaged quark amplitudes

$$U(s,b) = \prod_{Q=1}^{N} \langle f_Q(s,b) \rangle, \tag{9}$$

in accordance with the assumed quasi-independent nature of valence quark scattering.

The $b$–dependence of the function $\langle f_Q \rangle$, related to the quark formfactor $F_Q(q)$, has a simple form $\langle f_Q \rangle \propto \exp(-m_Q b/\xi)$.

Following the above considerations, the generalized reaction matrix in a pure imaginary case is represented in the form

$$U(s,b) = iG(N-1)^N \left[1 + \alpha\frac{\sqrt{s}}{m_Q}\right]^N \exp(-Mb/\xi), \tag{10}$$

where $M = \sum_{q=1}^{N} m_Q$, $G = \prod_{Q=1}^{N} g_Q$ and $\alpha = \kappa(1 - \langle x_Q\rangle)/(N-1)$. This expression allows one to get the scattering amplitude as a solution of Eq. 7, reproducing the main regularities observed in elastic scattering at small and large angles.

In the impact parameter representation the scattering amplitude may be written in the form:

$$F(s,b) = U(s,b)[1 - iU(s,b)]^{-1}. \tag{11}$$

This is the solution of Eq.7 at $s \gg 4m^2$. Note that the more familiar way to provide the direct channel unitarity consists in the representation of the scattering amplitude in the eikonal form

$$F(s,b) = \frac{i}{2}\left(1 - e^{i\chi(s,b)}\right),$$

where $\chi(s,b)$ is the eikonal function, related to the function $U(s,b)$ by the equation:

$$\chi(s,b) = i\ln\frac{1 - iU(s,b)}{1 + iU(s,b)}.$$

At moderate energies $s \ll s_0$, where $\sqrt{s_0} = m_Q/\alpha$ (note that the magnitude of $\alpha$ can be derived from the numerical analysis [3] and is about $1.5{\cdot}10^{-4}$, hence $\sqrt{s_0} \simeq 2$ TeV), the function $U(s,b)$ can be represented in the form

$$U(s,b) = i\tilde{g}\left[1 + N\alpha\frac{\sqrt{s}}{m_Q}\right]\exp(-Mb/\xi), \tag{12}$$

where $\tilde{g} = G(N-1)^N$. At very high energies $s \gg s_0$ we can neglect the energy independent term in Eq.10 and rewrite the expression for $U(s,b)$ as

$$U(s,b) = i\tilde{g}\left(s/m_Q^2\right)^{N/2}\exp(-Mb/\xi). \tag{13}$$

Calculation of the scattering amplitude is based on the impact parameter representation

$$F(s,t) = \frac{s}{2\pi^2}\int_0^\infty d\beta F(s,\beta)J_0(\sqrt{-\beta t}),\ \beta = b^2$$

and the analysis of singularities of $F(s,\beta)$ in the complex $\beta$–plane.

Besides the energy dependence of these observables, we will emphasize its dependence on geometrical characteristics of non–perturbative quark interactions.

The total cross–section has the following energy and quark mass dependencies:

$$\sigma_{tot}(s) = \frac{\pi\xi^2}{\langle m_Q\rangle^2}\Phi(s,N), \tag{14}$$

where $\langle m_Q\rangle = \frac{1}{N}\sum_{Q=1}^{N} m_Q$ is the mean value of the constituent quark masses in the colliding hadrons. The function $\Phi$ has the following behavior:

$$\Phi(s,N) = \begin{cases} (8\tilde{g}/N^2)\left[1 + N\alpha\sqrt{s}/m_Q\right], & s \ll s_0, \\ \ln^2 s, & s \gg s_0. \end{cases} \tag{15}$$

Thus, at asymptotically high energies the model provides

$$\lim_{s\to\infty}\frac{\sigma_{tot}(\bar{a}b)}{\sigma_{tot}(ab)} = 1.$$

The preasymptotic rise of the total cross–sections, linear with $\sqrt{s}$, is in agreement with the experimental data say up to $\sqrt{s} \sim 0.5$ TeV. In Fig.1–3 the dependence

$$\sigma_{tot} = A + B\sqrt{s} \tag{16}$$

is compared with the experimental data for $\bar{p}p$, $pp$, $K^{\pm}p$ and $\pi^{\pm}p$ interactions. It is interesting to note that these simple fits with two free parameters $A$ and $B$ indicate a possible intersection of particle and antiparticle total cross–sections, i.e. simulate the Odderon effect.

The inelastic cross-section can be calculated in the model explicitely, viz

$$\sigma_{inel}(s) = \frac{8\pi\xi^2}{N^2\langle m_Q\rangle^2}\ln\left[1 + \tilde{g}(1 + \frac{\alpha\sqrt{s}}{m_Q})^N\right]. \tag{17}$$

At asymptotically high energies the inelastic cross–section growth is as follows:

$$\sigma_{inel}(s) = \frac{4\pi\xi^2}{N\langle m_Q\rangle^2}\ln s. \tag{18}$$

At $s \gg s_0$ the dependence of the hadron interaction radius $R(s)$ and the ratio $\sigma_{el}/\sigma_{tot}$ on $s$ is given by the following equations:

$$R(s) \;=\; \frac{\xi}{2\langle m_Q\rangle}\ln s, \tag{19}$$

$$\frac{\sigma_{el}(s)}{\sigma_{tot}(s)} = 1 - \frac{4}{N \ln s}. \quad (20)$$

It is important to note here that such behavior of the ratio $\sigma_{el}/\sigma_{tot}$ and $\sigma_{inel}(s)$ is a result of the self–damping of inelastic channels [9] at small impact distances. Numerical estimates [3] show that the ratio $\sigma_{el}(s)/\sigma_{tot}(s)$ reaches the asymptotic value 1 at extremely high energy $\sqrt{s} = 500$ TeV.

Slower relative increase of the inelastic cross-section at high energies is due to the fact that the inelastic overlap function $\eta(s,b)$ becomes peripheral, and the whole picture corresponds to the antishadow scattering at $b < R(s)$ and to the shadow scattering at $b > R(s)$.

Such behavior of the contribution of inelastic channels arises because the scattering amplitude $f(s,b)$ goes beyond the black disc limit with the growth of energy:

$$|f(s,b)| > 1/2$$

at $b < R(s)$ [10]. The appearance of the region where the scattering process has antishadow nature is due to the self-damping of inelastic channels. Indeed, in the pure imaginary case $U(s,b)$ arises as a shadow of inelastic processes. However, the increase of the function $U(s,b)$ due to the increase of the contributions of inelastic channels leads to the decrease of inelastic overlap function at $b < R(s)$ and feedback the elastic channels. This behavior of the cross-sections is in accord with the lower bound for elastic cross-section [11]:

$$\sigma_{el}(s) > \left[\frac{\sigma_{tot}(s)}{36\pi g(s)}\right] \sigma_{tot}(s), \quad (21)$$

$$g(s) = \frac{d}{dt}(\ln \mathrm{Im}\, F(s,t))|_{t=0}.$$

The quantitative analysis of the experimental data [3] indicates that antishadow scattering mode starts to develop at $\sqrt{s} = 2$ TeV. This result is in agreement with the experimental indications from the CDF data that the elastic amplitude $f(s,b)$ at $b = 0$ already reaches the black disc limit [12]. The development of the antishadow mode in head-on $\bar{p}p$–collisions at Tevatron could be associated with new phenomena in the central hadronic collisions where the temperatures are high and the energy density can be up to several $GeV/fm^3$.

Thus, unitarization drastically changes the scattering picture: at lower energies inelastic channels provide dominant contribution and scattering amplitude has a shadow origin, while at high energies elastic scattering dominates over inelasic contribution and the scattering picture corresponds to the

antishadow mode. The functional $s$–dependencies of observables also differ significantly. For example, $s$–dependence of the total cross-section at $s \ll s_0$ is described by a simple linear function of $\sqrt{s}$. It has been shown that such dependence does not contradict the experimental data for hadron total cross–sections at least up to $\sqrt{s} \sim 0.5$ TeV (see Figs. 1-3 and [3] for earlier results). Such dependence corresponds to that of the hard Pomeron with $\Delta = 0.5$, however, it is obtained in a different approach [4]. This is the preasymptotic dependence and it has nothing to do with the true asymptotics of the total cross-sections. In the model such behavior of hadronic cross–sections reflects the energy dependence of the number of virtual quarks, generated in the intermediate transient stage of hadronic interaction.

The experimental data on $\sigma_{tot}(\gamma p)$ can also be described by Eq.16. The comparison with the data is given in Fig. 4. New data from HERA at small $x$ correspond to the c.m. energy range of $\gamma^* p$ system $W = 50 - 300$ GeV which, judging by the hadronic cross–sections behavior, should be considered as the preasymptotic energy region. In this region the rise of hadronic cross-sections is consistent with the linear dependence on $\sqrt{s}$.

The observed behavior of the structure function $F_2$ at small $x$ or, equivalently, the dependence of $\sigma_{tot}(\gamma^* p)$ on $W$ [2] favors Eq. 16 with $Q^2$-dependent parameters $A$ and $B$ (cf. Fig. 19 in [2], ZEUS data). In the framework of the model [4] we can speculate that this $Q^2$–dependence reflects the fact that the efficiency of the transformation of hadron kinetic energy into the masses of virtual quarks (parameter $\kappa$ in Eq. 5) depends on $Q^2$, $\kappa \to \kappa(Q^2)$, and the function $\kappa(Q^2)$ has the critical behavior with $Q^2$, viz it has a steep increase at $Q^2 \sim 1$ GeV$^2$. Thus, it seems premature to claim that the hadronic data and data obtained in deep-inelastic scattering require two Pomerons – soft and hard ones [13].

**Acknowledgement**

We are grateful to V.A. Petrov for interesting discussions.

# References


[1] E. A. Kuraev, L. N. Lipatov and V. S. Fadin: Sov. Phys. JETP 45 (1977) 199; Ya. Ya. Balitsky and L. N. Lipatov: Sov. J. Nucl. Phys. 28 (1978) 822

[2] I. Abt et al., H1 Collaboration: Nucl. Phys. B407 (1993) 515;
M. Derrick et al., ZEUS Collaboration: preprint DESY 94-113;
compilation of cross-sections is given in A. Levy: preprint DESY 95-003

[3] S.M. Troshin, N.E.Tyurin and O.P. Yuschenko: Nuovo Cim. 91A (1986) 23

[4] S.M. Troshin and N.E. Tyurin: Nuovo Cim. 106A (1993) 327; Proc. of the Vth Blois Workshop on Elastic and Diffractive Scattering, Providence, Rhode Island, June 1993, p. 387; Phys. Rev. D49 (1994) 4427; Z. Phys. C 64 (1994) 311

[5] R.D. Ball: Int. Journal of Mod. Phys. A5 (1990) 4391

[6] M.M. Islam: Z. Phys. C 53 (1992) 253

[7] P. Carruthers and Minh Duong-Van: Phys. Rev. D28 (1983) 130

[8] A.A. Logunov, V.I. Savrin, N.E.Tyurin and O.A.Khrustalev: Teor. Mat. Fiz. 6 (1971) 157

[9] M. Baker and R. Blankenbecler: Phys. Rev. 128 (1962) 415

[10] S. M. Troshin and N. E. Tyurin: Phys. Lett. B316 (1993) 175

[11] S. W. McDawell and A. Martin: Phys. Rev. 135 (1964) 960

[12] S. Belforte, CDF Collaboration: Nuovo Cim. 107A (1994) 2085

[13] P. V. Landshoff: The Two Pomerons, Talk given at PSI school at Zuos, August 1994; M. Bertini, M. Giffon and E. Predazzi: Two Pomerons?, INFN 1995

**Figure captions**

**Fig. 1** Total cross–sections of $\bar{p}p$– and $pp$–interactions. Data from Tevatron at $\sqrt{s} = 1.8$ TeV beyond the preasymptotic region have not been included.

**Fig. 2** Total cross–sections of $\pi^{\pm}p$–interactions.

**Fig. 3** Total cross–sections of $K^{\pm}p$–interactions.

**Fig. 4** Total cross–section of $\gamma p$–interactions.

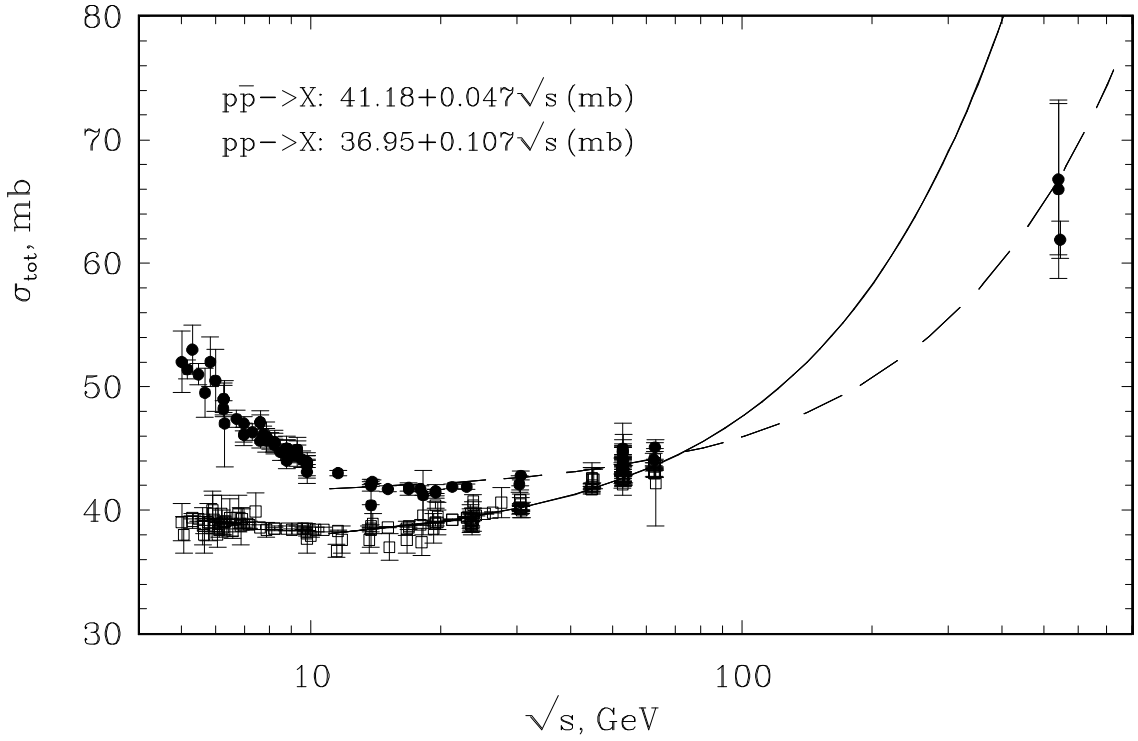
$p\bar{p}$->X: 41.18+0.047√s (mb)
pp->X: 36.95+0.107√s (mb)
$\sigma_{tot}$, mb
√s, GeV
80
70
60
50
40
30
10
100

Fig.1

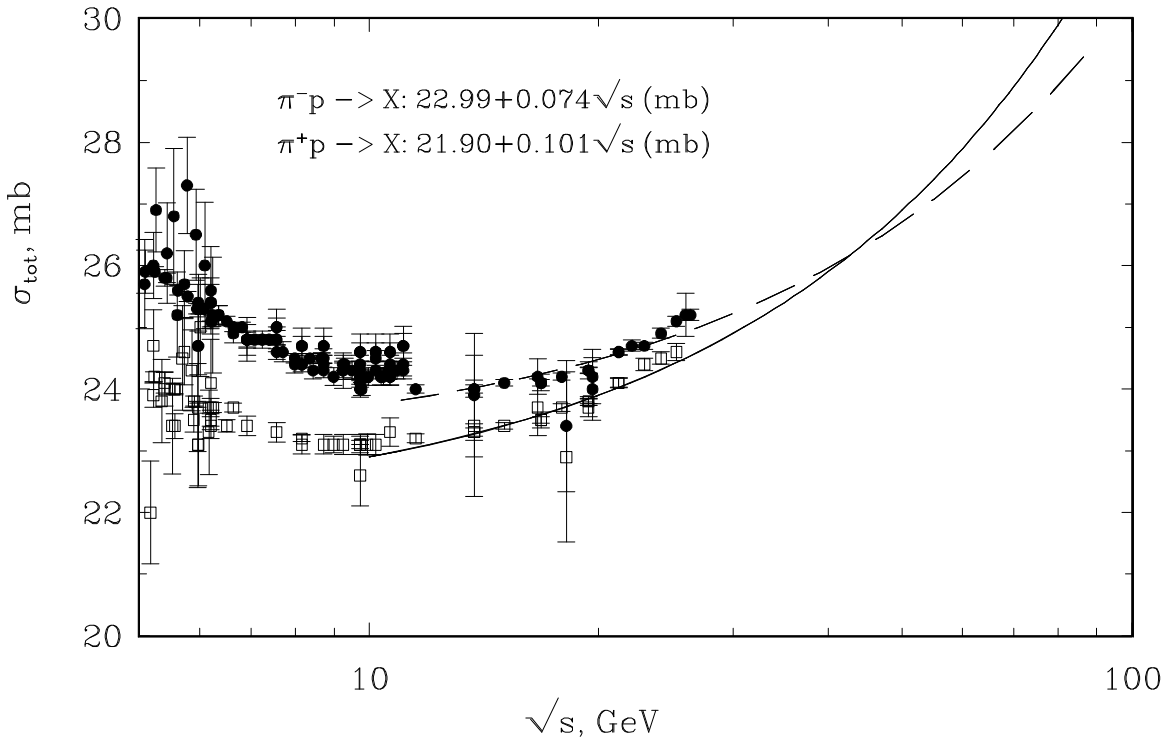
$\pi^-p$ -> X: 22.99+0.074√s (mb)
$\pi^+p$ -> X: 21.90+0.101√s (mb)
$\sigma_{tot}$, mb
√s, GeV
30
28
26
24
22
20
10
100

Fig.2

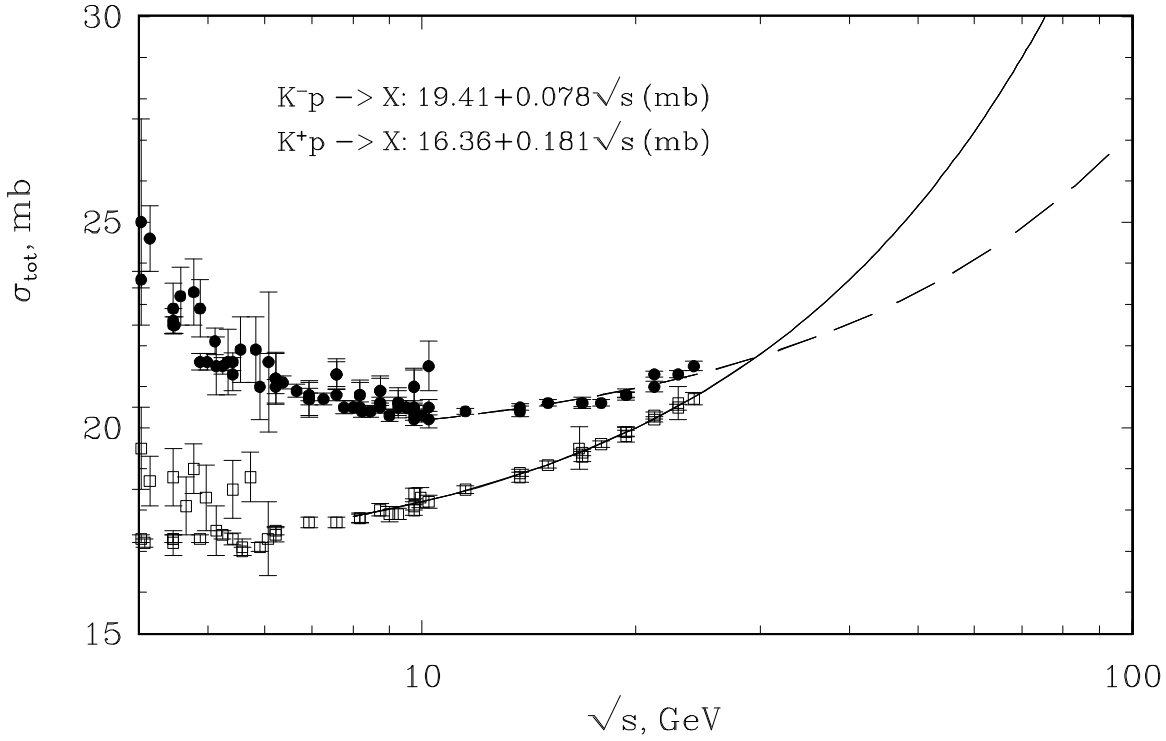
30
25
20
15
$\sigma_{tot}$, mb
$K^-p \rightarrow X$: 19.41+0.078$\sqrt{s}$ (mb)
$K^+p \rightarrow X$: 16.36+0.181$\sqrt{s}$ (mb)
10
100
$\sqrt{s}$, GeV

Fig.3

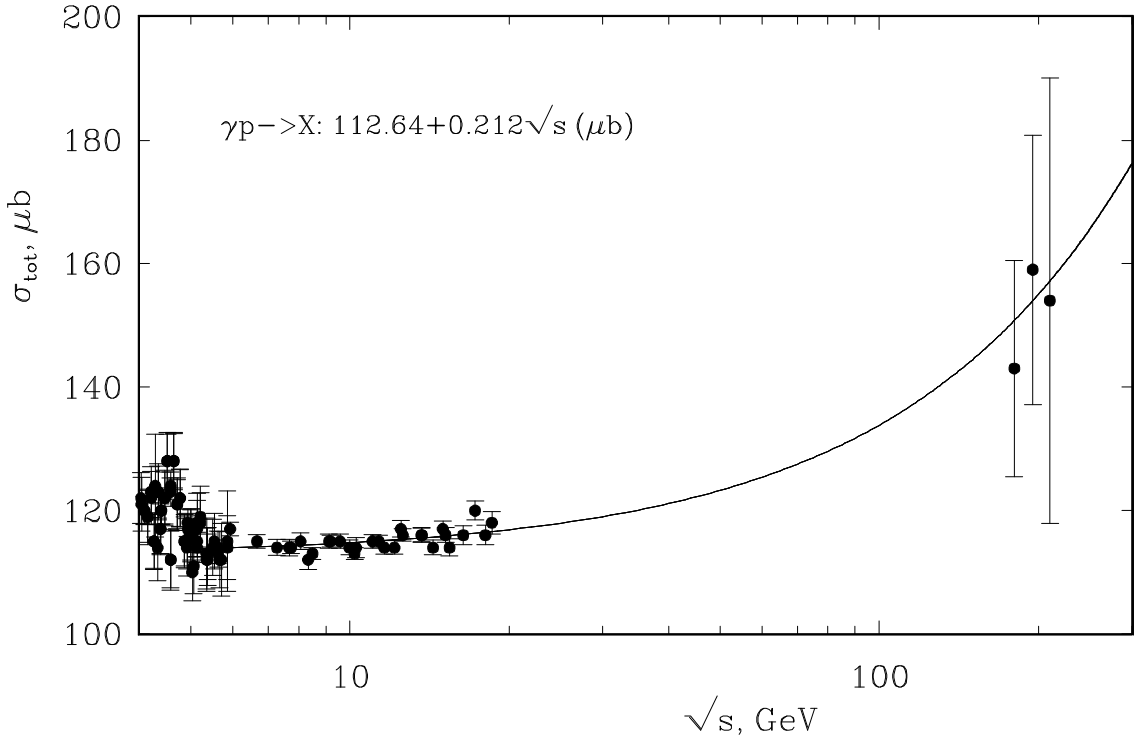
200
180
160
140
120
100
$\sigma_{tot}$, $\mu$b
$\gamma p \rightarrow X$: 112.64+0.212$\sqrt{s}$ ($\mu$b)
10
100
$\sqrt{s}$, GeV

Fig.4